Stabilization of Steady-State Drifting for a RWD Vehicle

Efstathios Velenis[1], Diomidis Katzourakis[2], Emilio Frazzoli[3], Panagiotis Tsiotras[4] and Riender Happee[2]

[1]**School of Engineering and Design, Brunel University, UK**
[2]**Biomechanical Engineering Research Group, Technical University of Delft, The Netherlands**
[3]**Department of Aeronautics and Astronautics, Massachusetts Institute of Technology, USA**
[4]**Daniel Guggenheim School of Aerospace Engineering, Georgia Institute of Technology, USA**

School of Engineering and Design, Brunel University
Uxbridge Middlesex, UB8-3PH, UK
Phone: +44 (0) 1895 267589
Fax: +44 (0) 1895 256392
E-mail: efstathios.velenis@brunel.ac.uk

We present data of driver control commands and vehicle response during the execution of cornering maneuvers at high sideslip angles (drifting) by an expert driver using a RWD vehicle. The data reveal that stabilization of the vehicle with respect to such cornering equilibria requires a combination of steering and throttle regulation. A four wheel vehicle model with nonlinear tire characteristics is introduced and the steady-state drifting conditions are solved numerically to derive the corresponding control inputs. A sliding mode control is proposed to stabilize the vehicle model with respect to steady-state drifting, using steering angle and drive torque inputs. The performance of the controller is validated in a high fidelity simulation environment.

Topics / Vehicle Control; Driver Behaviour and Driver Model; Vehicle Dynamics

1. Introduction

Recently, numerous studies on the dynamic behavior and control of vehicles considering their full handling capacity along with the operation of the tires in their nonlinear region have appeared in the literature. It is envisioned that a new generation of active safety systems will employ expert driving skills, instead of restricting the vehicle's response within the predictable linear region of operation of the tires, to actively maneuver vehicles away from accidents. A mathematical analysis of expert driving techniques was initiated in [1], [2], [3]. The driving techniques investigated in the above references using numerical optimization were those used by rally drivers, and clearly involve operation of the vehicle outside the stable operation envelope enforced by current active safety/stability systems.

The analysis in [1], [2], [3] provided a significant understanding of the dominant effects during execution of expert driving techniques, but the open-loop nature of the numerical optimization approach is not implementable in the presence of uncertainties. Several studies have appeared in the literature recently, contributing to a closed loop formulation of vehicle cornering at high sideslip angles. Derivation of steady-state cornering equilibria with the tires operating in their nonlinear region, a stability analysis using phase-plane techniques and the design of a robust stabilizing steering controller, neglecting the longitudinal forces (tractive or braking) at the tires, appeared in [4]. High sideslip angle (drifting) steady-state cornering conditions were derived in [5] using the lateral dynamics of a four wheel rear-wheel-drive (RWD) vehicle model and a combined traction/cornering tire friction model. The stability of steady-state drifting using a rich four wheel RWD vehicle model, incorporating longitudinal and lateral dynamics, load transfer effects and a combined motion tire friction model, was discussed in [6]. Derivation of drifting equilibria using vehicle models of lower order, and hence more appropriate for control design, were discussed in [7] and [8].

In addition to the steering controller in [4], stabilization of drifting equilibria appeared in [9] and [10]. In [9] a sliding mode control, using independent front and rear wheel drive/brake torque inputs, and assuming a fixed steering angle at its steady-state value, was designed to stabilize a single-track vehicle model with respect to drifting equilibria. In [10] a steering controller based on the lateral dynamics of a single-track model was implemented on an autonomous vehicle platform to perform steady-state drifting, while a separate speed controller was used to regulate the speed to the desired steady-state value.

In this work we present a controller to stabilize a RWD vehicle with respect to drifting equilibria,

based on a rich vehicle dynamics model, and using coupled lateral (steering) and longitudinal (drive torque) control inputs. We first present the results of a data collection experiment during the execution of steady-state drifting by an expert driver and discuss the driver steering, brake and throttle commands during the stabilization of the vehicle. We introduce a four wheel vehicle model, incorporating nonlinear tire friction characteristics, longitudinal and lateral load transfer effects and coupling of the rear wheels drive torques through modelling of a differential system. Using the four wheel model we calculate numerically the steady-state tire friction forces and the associated drive torque and steering angle control inputs corresponding to drifting equilibria. A linear controller is designed to stabilize the vehicle with respect to drifting equilibria using front wheel steering angle and rear wheel slip ratios (or equivalently rear wheel rotation rates). A sliding mode control scheme is then employed providing the drive torque input necessary to regulate the rear wheel speeds to the values dictated by the above linear controller. Finally, the control scheme is implemented in a high-fidelity simulation environment.

2. Data Analysis

In this section we present data of driver control inputs and corresponding vehicle response collected during the execution of a drifting maneuver by an experienced rally race driver. The data collection took place at the facilities of the Bill Gwynne Rally School in Brackley, UK, using a rally-race prepared 1980 1.6lt, 110bhp engine Ford Escort with a RWD transmission and a limited slip differential (Fig. 1). The vehicle vector velocity and sideslip angle were measured using a VBox twin GPS antenna sensor at 20Hz. An inertial measurement unit was placed close to the estimated location of the vehicle's C.M. to measure 3-axis body accelerations and 3-axis body rotation rates. Externally fitted optical encoders were used to measure the rotational speed of each individual wheel. A string potentiometer was used to measure the steering angle at the steering wheel, and a rotational potentiometer was fitted on the throttle pedal to measure the pedal position. The vehicle was fitted with two brake pressure sensors at the front and rear pairs of wheels. The data was collected using a purpose-built data logger at 100Hz. The driver executed drifting maneuvers on a loose surface (dirt on tarmac), aiming at maintaining approximately constant speed and sideslip angle along a path of approximately constant radius.

In Fig. 2 we present data for the vehicle states, namely, vehicle speed V, sideslip angle β, yaw rate $\dot{\psi}$ and individual wheel speeds ω_{ij}, $i = F$ (Front), R (Rear), $j = L$ (Left) , R (Right), during stabilization of the vehicle at a steady-state clockwise trajectory of radius approximately 13 m. The vehicle sideslip and yaw rate are positive along the counterclockwise direction. In the same figure we also present the corresponding driver inputs, namely, the steering angle of the front wheels, with positive values corresponding to turning the steering wheel to the left, as well as the normalized throttle pedal position, and normalized front and rear axle brake pressures. Part of the vehicle trajectory is shown in Fig. 3.

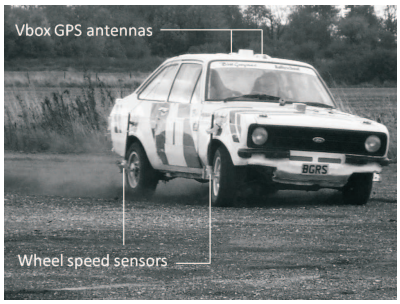

Figure 1: *The rally car used for data collection.*

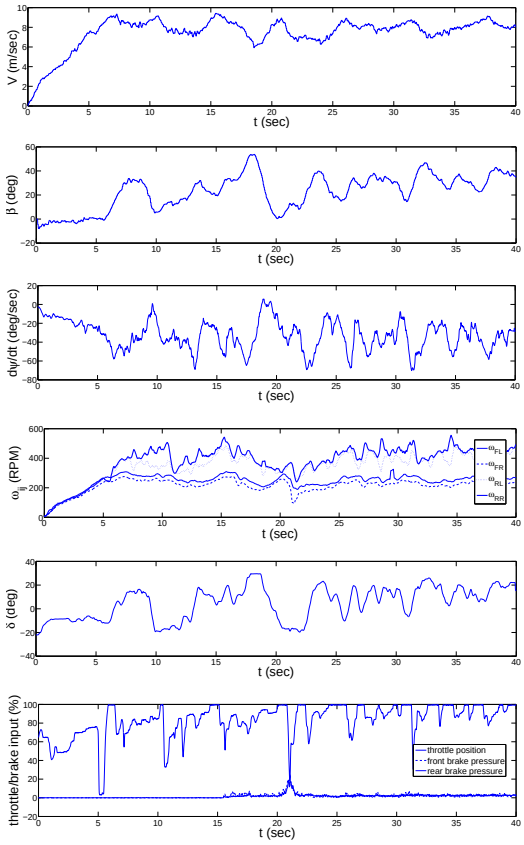

Figure 2: *Vehicle states and driver input data.*

Throughout the 13 m radius trajectory the driver applied no brake command, except from a small value during a brief interval around $t = 20$ sec. The vehicle started from standstill and accelerated while cornering to the right. Between $5 \leq t \leq 10$sec the vehicle developed a high sideslip angle of approximately 30 deg. At the beginning of this interval we notice application of full throttle, which resulted in the rear wheels to rotate at a considerably higher rate than the front ones. Hence the slip ratio at the rear wheels was increased and the rear cornering forces decreased (in accordance to the combined traction/braking and cornering operation of a tire [11]). The vehicle sideslip and yaw rate increased and the

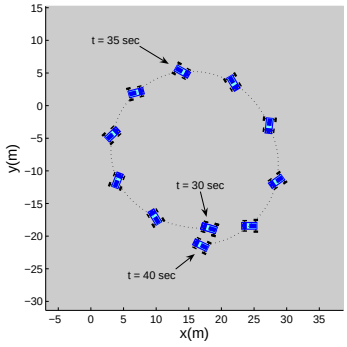

Figure 3: *Vehicle trajectory data.*

driver regulated the vehicle yaw moment by steering the front wheels towards the opposite direction with respect to the corner (counter-steered), while applying a high value of throttle input. Similarly, we notice peaks of sideslip angle at approximately $t = 13\,\text{sec}$ and $t = 17.5\,\text{sec}$ under high throttle commands and counter-steer. During $25 \leq t \leq 40\,\text{sec}$ we notice that the vehicle speed was stabilized close to 8.1 m/sec and the yaw rate close to 36 deg/sec. The sideslip angle is stabilized at approximately 32 deg. We notice that the driver applied throttle close to the maximum and consistently counter-steered. Despite the corrections in the control inputs by the driver and the fluctuations of the vehicle states in this interval, we consider that the vehicle achieved a steady-state cornering condition, characterized by a high sideslip angle, which is referred to as steady-state drifting or powerslide [6].

3. Vehicle Model

The equations of motion of a four-wheel vehicle, with front wheel steering, travelling on a horizontal plane (Fig. 4) are given below:

$$\begin{aligned} m\dot{V} &= (f_{FLx} + f_{FRx})\cos(\delta - \beta) \\ &- (f_{FLy} + f_{FRy})\sin(\delta - \beta) \\ &+ (f_{RLx} + f_{RRx})\cos\beta \\ &+ (f_{RLy} + f_{RRy})\sin\beta, \qquad (1) \\ \dot{\beta} &= \frac{1}{mV}\left[(f_{FLx} + f_{FRx})\sin(\delta - \beta)\right. \\ &+ (f_{FLy} + f_{FRy})\cos(\delta - \beta) \\ &- (f_{RLx} + f_{RRx})\sin\beta \\ &+ \left.(f_{RLy} + f_{RRy})\cos\beta\right] - \dot{\psi}, \qquad (2) \\ I_z\ddot{\psi} &= \ell_F\left[(f_{FLy} + f_{FRy})\cos\delta\right. \\ &+ \left.(f_{FLx} + f_{FRx})\sin\delta\right] \\ &+ w_L\left(f_{FLy}\sin\delta - f_{FLx}\cos\delta - f_{RLx}\right) \\ &+ w_R\left(f_{FRx}\cos\delta - f_{FRy}\sin\delta + f_{RRx}\right) \\ &- \ell_R\left(f_{RLy} + f_{RRy}\right), \qquad (3) \\ I_w\dot{\omega}_{ij} &= T_{ij} - f_{ijx}r \;\; (i = F, R,\; j = L, R). \qquad (4) \end{aligned}$$

In the above equations m is the vehicle's mass, I_z is the moment of inertia of the vehicle about the vertical axis, V is the vehicle velocity at the center of mass (C.M.), β is the sideslip angle at the C.M. and ψ is the yaw angle. The moment of inertia of each wheel about its axis of rotation is I_w, the radius of each wheel is r, and the rotation rate of each wheel is ω_{ij} $(i = F, R,\; j = L, R)$. The steering angle of the front wheels (assuming equal angle for left and right front wheels) is denoted by δ, and the drive/brake torque applied on each wheel is T_{ij}. We have neglected the rolling resistances and self-aligning moments at the tires. The longitudinal and lateral friction forces at each wheel are denoted by f_{ijk} $(i = F, R,\; j = L, R$ and $k = x, y)$. The distances ℓ_F, ℓ_R, w_L and w_R determine the location of the C.M. with respect to the center of each wheel, as in Fig. 4.

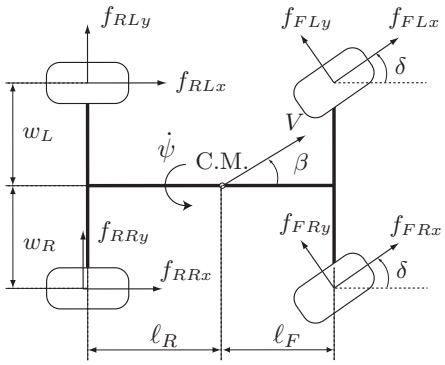

Figure 4: *Full-car vehicle model.*

The tire forces f_{ijk} in the above vehicle model are calculated as functions of tire slip and wheel normal load using Pacejka's Magic Formula [11]. Tire slip refers to the non-dimensional relative velocity of the tire with respect to the road. The slip ratio and lateral slip [11] are defined as:

$$s_{ijx} = \frac{V_{ijx} - \omega_{ij}r_{ij}}{\omega_{ij}r_{ij}}, \qquad s_{ijy} = \frac{V_{ijy}}{\omega_{ij}r_{ij}}, \qquad (5)$$

respectively, where V_{ijk} $(i = F, R,\; j = L, R,\; k = x, y)$ are the tire frame components of the vehicle velocity vector at the centers of the four wheels.

Neglecting vertical motion and pitch and roll rotations of the sprung mass of the vehicle, we calculate the normal load at each of the four wheels considering the static load distribution and longitudinal/lateral normal load transfer under longitudinal/lateral acceleration. For instance, acceleration a_x along the longitudinal body axis results in load transfer from front to rear wheels as follows:

$$\Delta f^x = \frac{m\,h\,a_x}{\ell_F + \ell_R}, \qquad (6)$$

where h is the distance of the vehicle's C.M. from the road level. Similarly, acceleration a_y along the lateral body axis results in load transfer from front-left to front-right and rear-left to rear-right wheels.

Finally, we introduce the model of a limited slip differential (LSD) system, which provides coupling of the drive torques of the driven rear-left and rear-right wheels, and allows us to consider a single drive torque input, corresponding to the driver's throttle

command. Considering a RWD vehicle and assuming no braking command we have front wheel torques $T_{Fj} = 0$, $(j = L, R)$. The output drive torque T_R from the gearbox will then be distributed between the rear-left and rear-right wheels, providing T_{RL} and T_{RR} of equation (4). In this work we use the torque transfer characteristics of a LSD differential model of the CarSim vehicle simulation software [12]. In particular, the torque transfer as a function of the wheel speed differential is provided in CarSim in the form of a look-up table. The data of the look-up table were used to identify the following explicit expression of the differential torque transfer as a function of the wheel speed differential (Fig. 5):

$$\Delta T(\Delta\omega) = -\text{sign}(\Delta\omega) C_d \sqrt{|\Delta\omega|}, \tag{7}$$

where $\Delta T = T_{RL} - T_{RR}$, $\Delta\omega = \omega_{RL} - \omega_{RR}$, and C_d is a positive constant. We may now consider a single torque input $T_R = T_{RL} + T_{RR}$ corresponding to the gearbox torque output, providing rear-left and rear-right wheel torques as follows:

$$T_{RR} = \frac{T_R - \Delta T(\Delta\omega)}{2}, \; T_{RL} = \frac{T_R + \Delta T(\Delta\omega)}{2}, \tag{8}$$

where $\Delta T(\Delta\omega)$ from (7). Finally, using equations (4), (7) we derive the dynamics of the rear wheels speed differential as follows:

$$I_w \frac{\mathrm{d}\Delta\omega}{\mathrm{d}t} = \Delta T(\Delta\omega) - (f_{RLx} - f_{RRx}) r. \tag{9}$$

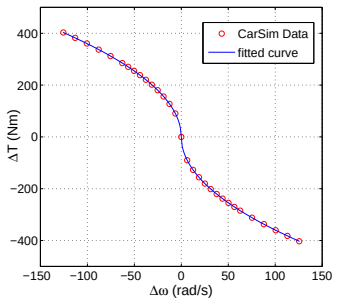

Figure 5: *LSD torque transfer characteristic.*

4. Steady-State Cornering Conditions

Steady-state cornering is characterized by a trajectory of constant radius $R = R^{\text{ss}}$, negotiated at a constant speed $V = V^{\text{ss}}$, constant yaw rate $\dot{\psi} = \dot{\psi}^{\text{ss}} = V^{\text{ss}}/R^{\text{ss}}$, constant sideslip angle $\beta = \beta^{\text{ss}}$, and constant wheel rotation rates $\omega_{ij} = \omega_{ij}^{\text{ss}}$. In steady-state cornering the control inputs, namely the steering angle $\delta = \delta^{\text{ss}}$ and rear axle torque $T_R = T_R^{\text{ss}}$ also remain constant.

Enforcing a steady-state cornering condition:

$$\dot{V} = 0, \qquad \dot{\beta} = 0, \qquad \ddot{\psi} = 0, \qquad \dot{\omega}_{ij} = 0, \tag{10}$$

considering a RWD transmission and no braking command (in accordance to the data), that is enforcing free rolling of the front wheels:

$$s_{Fjx}^{\text{ss}} = 0, \quad f_{Fjx}^{\text{ss}} = 0, \quad T_{Fj}^{\text{ss}} = 0, \quad j = L, R, \tag{11}$$

and providing fixed values for the steady-state pair $(R^{\text{ss}}, \beta^{\text{ss}})$, we are able to solve numerically equations (1)-(8) for the rest of the steady-state state variables V^{ss}, ω_{ij}^{ss}, steady-state slip quantities and tire forces s_{ijk}^{ss}, f_{ijk}^{ss}, normal loads at the wheels f_{ijz}^{ss}, and steady-state control inputs δ^{ss} and T_R^{ss}.

In Fig. 6 we present cornering equilibria for a range of path radius R^{ss} and sideslip angle β^{ss}, considering the vehicle and tire model parameters of Table 1. In particular, we have plotted the steady-state value of the centripetal acceleration $a_{\text{cent}}^{\text{ss}} = (V^{\text{ss}})^2/R^{\text{ss}}$, and the solid line passes through the maximum $a_{\text{cent}}^{\text{ss}}$ for fixed R^{ss}. We notice the existence of steady-state conditions at extremely low path radii, which may expand the mobility characteristics of the vehicle, and that along paths of low radii the vehicle achieves the highest speed equilibria at higher sideslip angles. These observations will be further examined as part of our future work.

Table 1: *Estimated test-vehicle parameters.*

m (kg)	850	ℓ_F (m)	1.25
I_z (kgm^2)	1400	ℓ_R (m)	1.25
I_w (kgm^2)	0.6	r (m)	0.311
w_L, w_R (m)	0.74	B	4
C_d (Nm/(rad/s)$^{1/2}$)	35.949	C	1.3
h (m)	0.5	D	0.62

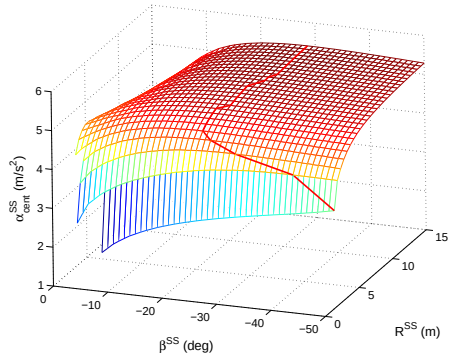

Figure 6: *Calculated steady-state equilibria.*

In Table 2 the steady-state condition achieved during the data collection experiment is compared to a calculated steady-state condition using the four-wheel vehicle model. We notice that, despite the uncertainty in many of the vehicle and tire parameters, the calculated steady-state closely matches the data.

5. Stabilization of Steady-State Cornering

In the following we propose a control scheme to stabilize a RWD vehicle with respect to drifting equilibria, using control inputs directly correlated to the driver's commands. The proposed architecture consists of a linear controller providing stabilizing front wheel steering angle (corresponding to the driver's steering command), and rear wheel slip ratio inputs.

Table 2: *Steady-state drifting condition.*

Variable	Data	Calculated
$V^{\rm ss}$ (m/sec)	8.1	8.35
$\lvert\beta^{\rm ss}\rvert$ (deg)	31.4	32
$\lvert\dot{\psi}^{\rm ss}\rvert$ (deg/sec)	36	36.8
$\lvert\Delta\omega^{\rm ss}\rvert$ (RPM)	42.7	64.2
$\lvert\delta^{\rm ss}\rvert$ (deg)	12.5	13.8

In addition, a sliding mode controller calculates the rear differential drive torque necessary for the rear-left and rear-right wheels to achieve the slip ratios dictated by the previous linear controller.

Neglecting the dynamics of rotation of each individual wheel (4), we express the equations of motion of the full-car model (1)-(3), including the rear wheel speed differential equation (9), as a system driven by the control inputs δ and one of the rear-left or rear-right wheel slip ratios, for instance s_{RRx}:

$$\dot{\tilde{x}} = f(\tilde{x}, u), \tag{12}$$

where $\tilde{x} = [V\, \beta\, \dot{\psi}\, \Delta\omega]^T$ and $\tilde{u} = [s_{RRx}\, \delta]^T$. We notice that, given the state variables V, β and $\dot{\psi}$, the control input s_{RRx} can be used to calculate the rear-right wheel speed ω_{RR} from the definition (5). Then, using the state variable $\Delta\omega$, we calculate the rear-left wheel speed ω_{RL}, and rear-left wheel slip ratio s_{RLx} from (5). Hence, we may calculate longitudinal and lateral friction forces at both rear wheels, using the tire model of [11]. We also enforce free rolling of the front wheels (11).

Equations (12) are linearized about the equilibrium $\tilde{x}^{\rm ss} = [V^{\rm ss}\, \beta^{\rm ss}\, \dot{\psi}^{\rm ss}\, \Delta\omega^{\rm ss}]^T$ and $\tilde{u}^{\rm ss} = [s^{\rm ss}_{RRx}\, \delta^{\rm ss}]^T$ and a linear quadratic regulator is designed

$$\tilde{u} - \tilde{u}^{\rm ss} \;=\; -\mathcal{K}(\tilde{x} - \tilde{x}^{\rm ss}), \tag{13}$$

to stabilize the system (12) with respect to the equilibrium $\tilde{x}^{\rm ss}$, using steering angle and rear-right wheel slip ratio inputs.

Next, we design a sliding mode controller using the rear drive torque T_R to regulate the slip ratios of the rear wheels to the values generated by the control law (13). We define the variable $\tilde{z}_{RR}$ as the difference between the actual wheel angular rate ω_{RR} and a reference wheel angular rate corresponding to a reference value of longitudinal slip $\hat{s}_{RRx}(V, \beta, \dot{\psi}, \Delta\omega)$:

$$\tilde{z}_{RR} = \omega_{RR} - \phi_{RR}(V, \beta, \dot{\psi}, \Delta\omega), \tag{14}$$

where $\phi_{RR}(V, \beta, \dot{\psi}, \Delta\omega)$ is the value of wheel rotation rate corresponding to the longitudinal slip $\hat{s}_{RRx}$ generated by (13):

$$\phi_{RR}(V, \beta, \dot{\psi}, \Delta\omega) = \frac{V_{RRx}}{(1 + \hat{s}_{RRx}(V, \beta, \dot{\psi}, \Delta\omega))r}.$$

The sliding mode controller generates the following rear-right wheel torque

$$T_{RR} = T^{\rm eq}_{RR} + I_w \hat{v}_{RR}, \tag{15}$$

where

$$\begin{aligned} T^{\rm eq}_{RR} \;&=\; f_{RRx} r + I_w \left(\frac{\partial \phi_{RR}}{\partial V} f_1 + \frac{\partial \phi_{RR}}{\partial \beta} f_2 \right. \\ &+ \left. \frac{\partial \phi_{RR}}{\partial \dot{\psi}} f_3 + \frac{\partial \phi_{RR}}{\partial \Delta\omega} f_4 \right). \end{aligned} \tag{16}$$

The component $T^{\rm eq}_{RR}$ is referred to as the *equivalent control*. Taking $T_{RR} = T^{\rm eq}_{RR}$ results in $\dot{\tilde{z}}_{RR} = 0$ and ensures that the vehicle's states will remain in the *sliding manifold* $\tilde{z}_{RR} = 0$. Equations (4), (14), (15) and (16) yield

$$\dot{\tilde{z}}_{RR} = \hat{v}_{RR}. \tag{17}$$

Finally, we take

$$\hat{v}_{RR} = -\lambda_{RR} \mathrm{sat}(\tilde{z}_{RR}), \quad \lambda_{RR} > 0. \tag{18}$$

It can be readily shown that the control (18) stabilizes (17) [13]. In fact, all trajectories starting off the *sliding manifold* $\tilde{z}_{RR} = 0$ will reach it in finite time under the control input (15). We notice that given T_{RR} from (15) we can calculate the corresponding rear differential drive torque T_R and rear-left wheel torque T_{RL} from equations (8).

6. Simulation Results

In the following we present the implementation of the control scheme of the previous section in simulation. The parameters of the vehicle and tire friction model used in the numerical calculations are summarized in Table 1, and we consider stabilization with respect to the calculated steady-state condition of Table 2. The initial velocity is perturbed by 30% and the initial sideslip angle by 50% from their steady-state values. The vehicle states and control inputs are shown in Fig. 7. The states and inputs corresponding to the simulation of the full-car model (1)-(3), (4) with static normal load transfer (6), are denoted as "no suspension". The controller (13), (15) successfully stabilizes the vehicle with respect to the corresponding cornering equilibrium in finite time.

To further validate the control architecture, we implement the sliding mode controller using CarSim to simulate the response of a high-fidelity vehicle model including suspension dynamics. For consistency we incorporate the same tire friction model as with the "no suspension" model. We observe that the responses of the two different models are very close, and that the suspension dynamics essentially have no effect on the performance of the controller. We recall that the steady-state equilibria were derived after neglecting the suspension dynamics. Figure 8 shows the trajectory of the vehicle during stabilization, generated by the animation tool of CarSim.

7. Conclusions

In this work we studied the stabilization of RWD vehicles with respect to cornering equilibria characterized by aggressive sideslip angles. We discussed the results of a data collection experiment during execution of steady-state drifting by an expert driver

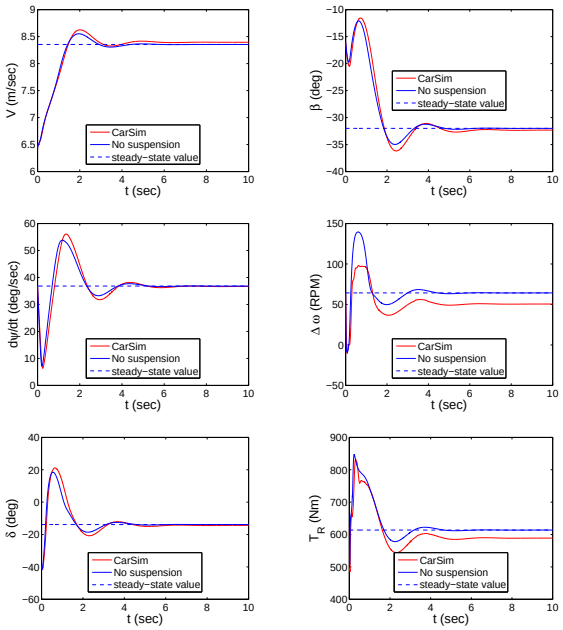

Figure 7: *Vehicle states and control inputs during stabilization with respect to the cornering equilibrium of Table 2.*

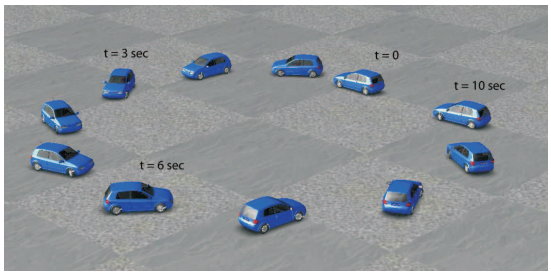

Figure 8: *Vehicle trajectory during stabilization.*

and concluded that RWD vehicle drifting stabilization requires a combination of throttle and steering regulation. A full-car vehicle model with nonlinear tire characteristics was introduced to numerically calculate the steady-state cornering states and inputs. Incorporating realistic drive-train modelling we were able to derive control input variables with direct correlation to the driver's steering and throttle commands, namely, the steady-state front wheel steering angle and rear differential drive torque. A sliding mode control scheme was then proposed to stabilize the vehicle with respect to drifting cornering equilibria. The controller used combined steering angle and drive torque inputs, in accordance to our experimental observations, and was successfully validated via implementation in a high fidelity simulation environment.

Acknowledgements

The work of E. Velenis was supported by a Marie Curie International Reintegration Grant within the 7th European Community Framework Programme, and a Brunel University BRIEF award. The work of E. Frazzoli was supported by ARO award W911NF-07-1-0499. The work of P. Tsiotras was supported by ARO award no W911NF-05-1-0331 and NSF GOALI award no CMMI-0727768.

REFERENCES

[1] E. Velenis and P. Tsiotras, "Minimum time vs maximum exit velocity path optimization during cornering," in *2005 IEEE International Symposium on Industrial Electronics*, Dubrovnic, Croatia, June 2005, pp. 355–360.

[2] E. Velenis, P. Tsiotras, and J. Lu, "Modeling aggressive maneuvers on loose surfaces: The cases of trail-braking and pendulum-turn," in *Proceedings of the 2007 European Control Conference*, Kos, Greece, July 2-5 2007.

[3] ——, "Optimality properties and driver input parameterization for trail-braking cornering," *European Journal of Control*, vol. 14, no. 4, pp. 308–320, July-August 2008.

[4] E. Ono, S. Hosoe, H. Tuan, and S. Doi, "Bifurcation in vehicle dynamics and robust front wheel steering control," *IEEE Transactions on Control Systems Technology*, vol. 6, no. 3, pp. 412–420, May 1998.

[5] M. Abdulrahim, "On the dynamics of automobile drifting," in *SAE World Congress*, Detroit, MI, April 3-6 2006.

[6] J. Edelmann and M. Plöchl, "Handling characteristics and stability of the steady-state powerslide motion of an automobile," *Regular and Chaotic Dynamics*, vol. 14, no. 6, pp. 682–692, 2009.

[7] E. Frazzoli, "Discussion on "Optimality Properties and Driver Input Parameterization for Trail-Braking Cornering"," *European Journal of Control*, vol. 14, no. 4, July-August 2008.

[8] R. Hindiyeh and J. Gerdes, "Equilibrium analysis of drifting vehicles for control design," in *Proceedings of the ASME 2009 Dynamic Systems and Control Conference*, Hollywood, CA, USA, October 12-14 2009.

[9] E. Velenis, E. Frazzoli, and P. Tsiotras, "On steady-state cornering equilibria for wheeled vehicles with drift," in *48th IEEE Conference on Decision and Control*, Shanghai, China, December 16-18 2009.

[10] C. Voser, R. Hindiyeh, and J. Gerdes, "Analysis and control of high sideslip maneuvers," in *21st International Symposium on Dynamics of Vehicles on Roads and Tracks*, Stockholm, Sweden, August 17-21 2009.

[11] E. Bakker, L. Nyborg, and H. Pacejka, "Tyre modelling for use in vehicle dynamics studies," 1987, SAE Paper No. 870421.

[12] *CarSim User Manual*. Mechanical Simulation Corp., Ann Arbor, MI, 2009.

[13] H. Khalil, *Nonlinear Systems, 2nd edition*. Upper Saddle River, New Jersey: Prentice Hall, 1996.